Analysis of Unsteady Pressures Induced on a Body by a Rotor

Nai-pei Bi* and J. G. Leishman†
University of Maryland, College Park, Maryland 20742

An analysis was conducted on the unsteady pressures measured on a body surface in proximity to a rotor. Unsteady pressures were measured at strategic points on the body in forward flight at various combinations of advance ratio, rotor thrust, and tip-path-plane angle. It was found that the local values of unsteady pressure were significantly altered by small changes in rotor thrust and advance ratio; tip-path-plane angle variations had a much smaller effect. Four characteristic pressure signatures representative of 1) blade passage, 2) close wake interactions with the body, 3) wake impingement on the body, and 4) postwake impingement were distinguished. These classifications were supported by correlations with shadowgraphic flow visualization of the rotor wake/body interaction, as well as unsteady potential flow models. This general classification of the surface pressure signatures has permitted a greater physical understanding of the overall air loads and possible mechanisms responsible for the interactional effects between a helicopter rotor and its fuselage.

Nomenclature

b = number of blades
C_p^u = unsteady pressure coefficient, $100(p^u - p_\infty)/(\frac{1}{2}\rho\Omega^2R^2)$
C_T = rotor thrust coefficient, $T/(\rho\pi\Omega^2R^2)$
c = blade chord
p_∞ = static pressure, Pa
p^u = unsteady component of pressure, Pa
R = rotor radius, m
T = rotor thrust, N
t = time, s
V = local flow velocity, m/s
V_∞ = tunnel freestream velocity, m/s
α_{TPP} = tip-path-plane angle of attack, deg
Γ = vortex strength, m^2/s
θ_c = collective pitch angle, deg
μ = advance ratio, $V_\infty/\Omega R$
ρ = air density, kg/m^3
σ = rotor solidity, $bc/\pi R$
ϕ = velocity potential
χ = wake skew angle, deg
ψ = blade azimuth angle, deg
Ω = rotor rotational frequency, rad/s

Introduction

THE understanding and prediction of the three-dimensional unsteady flowfield near a helicopter rotor and its fuselage is an extremely challenging problem. The rotor has several blades that are heavily loaded near their tips. As a result, the blades produce very strong tip vortices with somewhat weaker vortex sheets farther inboard. In forward flight, this wake system is convected below and trailed behind the rotor, and the vortices quickly evolve into a very complex three-dimensional flowfield structure. Reference 1 vividly illustrates the intricacy of this process.

In hover and low-speed forward flight, the rotor wake is transported almost vertically downward toward the helicopter fuselage and empennage, where the wake may directly impinge on aerodynamically important parts of the airframe. Thus, besides the unsteady loads induced on the fuselage by the passage of the rotating blades themselves over the fuselage, significant unsteady airloads are induced by the rotor wake system. These effects may lead to significant airframe vibrations that may prove detrimental to the airframe fatigue life, as well as the comfort of the occupants. The induced airloads may adversely affect the handling qualities of the aircraft, which sometimes require extensive flight tests to resolve.[2,3] Also, the airframe will distort the geometry of the rotor wake itself,[4] and this may have a considerable influence on the rotor inflow distribution[5] and net rotor performance. Such complicated effects are still the subject of considerable research on both theoretical and experimental fronts.

In the quest for more compact, lighter, and more maneuverable helicopters, current design trends often require the use of higher rotor disk loadings and smaller rotor/fuselage spacings.[4] The stronger tip vortices and higher downwash velocities intrinsically associated with highly loaded rotors mean that more severe aerodynamic interactions between the rotor and the fuselage may be produced. Thus, the understanding and prediction of interactional aerodynamic effects have become a more acute problem in helicopter design.

A fair amount of experimental and analytical research has been conducted to quantify the wake behavior and unsteady airloads near, and on, a helicopter fuselage. Fail and Eyre,[6] Makofski and Menkick,[7] and Payne[8] were some of the first investigators to conduct experiments to measure the airloads induced by a rotor on a flat plate immersed in a rotor wake. Sheridan and Smith[9] performed some pioneering work to quantify more completely the interactional aerodynamic loads between the components of a helicopter. Although the significance of unsteady effects was emphasized in Refs. 6–9, the aerodynamic mechanisms responsible for the airloads were not fully understood at this time.

Since then, several researchers have tackled the interactional problems in more detail. Efforts have been specifically aimed at a more complete understanding of the underlying physical processes of the interaction mechanisms. Wilson and Mineck[10] conducted tests to study the effects of rotor wake on the time-averaged aerodynamic characteristics of three different helicopter fuselage models. Considerable downloads and yawing moments were measured on the fuselage. Later, Betzina and Shinoda[11] and Smith and Betzina[12] conducted a series of wind-tunnel tests to investigate the time-averaged aerodynamic interactions for a simplified helicopter system consisting of a teetering two-bladed rotor and a body of revolution. However, these tests were conducted at advance ratios above 0.15 where the wake is skewed well above and does not impinge on the body. Nevertheless, they concluded that the rotor performance

Received Aug. 6, 1990; revision received Jan. 22, 1991; accepted for publication April 6, 1991.

*Graduate Research Assistant, Center for Rotorcraft Education and Research, Department of Aerospace Engineering.

†Assistant Professor, Center for Rotorcraft Education and Research, Department of Aerospace Engineering.

was significantly affected by the presence of the body and the aerodynamic characteristics of the body were highly modified by the presence of the rotor and its wake.

More recently, considerable attention has been placed on the measurement of the unsteady flowfield structure and related unsteady pressures on the fuselage. Experiments have been made by workers at the Georgia Institute of Technology to investigate the aerodynamic interactions between a cylindrical body and a two-bladed teetering rotor system.[13-25] Measurements of the instantaneous and time-averaged pressures on the cylinder surface were obtained at one representative rotor thrust. Velocity components at selected regions of the flowfield were also made using laser Doppler velocimetry (LDV) techniques. Laser sheet flow visualization of the vortex wake trajectories[25] complemented these measurements. Although results have helped to provide a much more comprehensive picture of the interactional mechanisms and an extensive data base for predictive code validation, it has still proved difficult to isolate the relative effects due to different interactional phenomena. This is particularly necessary for the validation of models of wake distortion and wake impingement on the airframe. Also, the important effects of rotor thrust variation and, therefore, blade loading and associated wake vortex strengths have not been thoroughly studied.

The complexity of the physics associated with rotor/airframe interactions has so far defied complete theoretical prediction. Many investigators, including Bramwell,[26] Clark and Maskew,[27,28] Freeman,[29] Lorber and Egolf,[30] Berry,[31] Rand,[32] Crouse et al.,[33] Quackenbush and Bliss,[34] and Brand et al.,[21] have assembled potential flow models of varying degrees of sophistication to help predict both the steady and unsteady surface pressures induced on the fuselage. Correlations with time-averaged pressure measurements have been reasonable. However, the prediction of unsteady effects has been somewhat less successful, except perhaps for blade passage effects.[23,33]

The unsteady effects induced by the rotor wake, particularly during wake impingement on the body, are poorly understood and are not easily modeled.[33,34] Furthermore, there are limited measurements available that can be used to guide the development of any semiempirical modeling of the wake impingement problem. Many existing measurements contain the combined effects of two or more interactional phenomena, from which it is difficult to isolate the contributions from events such as wake vortex impingement. Thus, one possible key to predicting the unsteady airloads on the fuselage is a more complete isolation of the various types of aerodynamic interactional phenomena that exist between the rotor, its wake, and the fuselage. It is also necessary to examine the important interrelated effects of rotor thrust, tip-path-plane angle of attack and advance ratio.

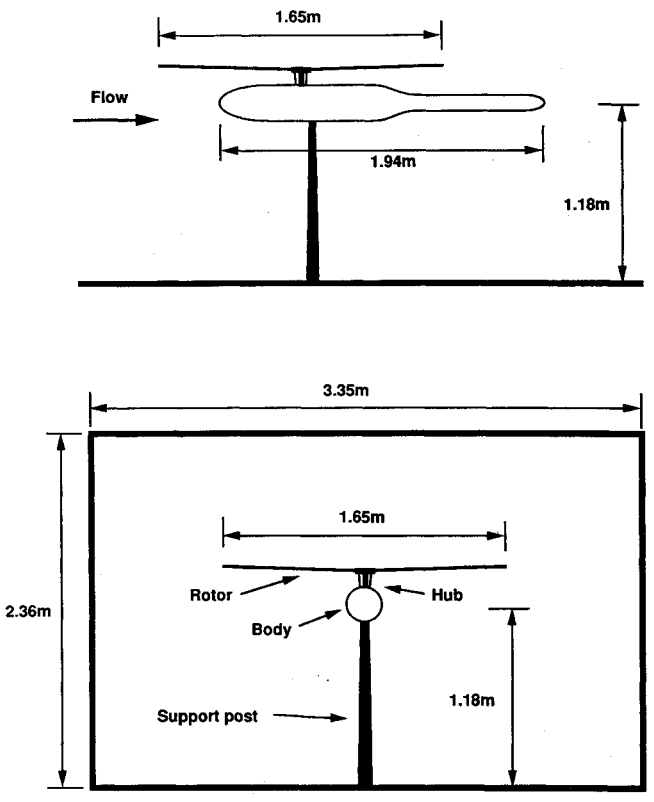

Fig. 1 Rotor and fuselage configuration.

This paper extends the work reported in Refs. 35 and 36. It is shown that the measurement of unsteady surface pressures at strategic points on the body can be used to build a more comprehensive understanding of the flowfield structure and the relative significance of the interactional mechanisms between a rotor and its fuselage. From the results of parametric studies, characteristic pressure signatures were classified and were attributed to different types of aerodynamic interactions with the body. These classifications are supported by means of flow visualization of the rotor wake using wide-field shadowgraphy, as well as theoretical methods based on unsteady potential flow models.

Description of the Experiment

The experiments were conducted in the University of Maryland's Glenn L. Martin wind tunnel, which is a closed-return tunnel with a 2.36×3.35-m working section. Figure 1 shows the general arrangement of the rotor/body system, which consisted of a 1.65-m-diam four-bladed rotor with a fully articulated hub and an idealized helicopter fuselage comprising a body of revolution. The body was 1.94 m long, the diameter of the main body was 0.254 m, and the diameter of the tail boom was 0.102 m. The spacing between the rotor plane and the centerline of the body was 0.24 m.

The rotor consisted of a fully articulated hub and conventional swash-plate arrangement. Power was supplied by a hydraulic motor. The rotor blades were of rectangular planform with a chord of 6.35 cm and with 12 deg of linear, nose down, twist. The blades consisted of a distribution of NASA RC(4)10 and RC(3)10 airfoil sections. The hub had a nominal radius (excluding blade pitch attachments) of 8% rotor radius and contained four coincident flap and lead-lag hinges. Rotor controls were comprised of the swash plate and pitch link mechanism; collective, lateral, and longitudinal cyclic pitch angles were set remotely by positioning the swash plate using three electromechanical actuators. The complete rotor and body assembly was mounted on a post that was hinged under the wind-tunnel floor. This allowed the whole rotor and body assembly to be tilted in unison using a hydraulic actuator.

In the tests, the tunnel-wind speed was slowly increased while the rotor was trimmed to the desired test condition by adjusting cyclic and collective pitch inputs to eliminate the 1/rev blade flapping response relative to the shaft. This is a standard approach for wind-tunnel testing of articulated rotors and ensures that the rotor tip path plane (TPP) is perpendicular to the rotor shaft axis. The centerline of the body was perpendicular to the rotor shaft axis; therefore, the TPP was parallel to the body centerline. Data were then recorded after reaching the desired thrust and advance ratio.

Instrumentation

A total of 21 temperature compensated piezoelectric pressure sensors were located at strategic points on the body, as shown in Figs. 2. These sensors were primarily concentrated over the nose and tail of the body, where significant interactional effects were expected. The outputs from the sensors were connected to a high-speed data acquisition system. The signals from each channel were amplified and then sampled simultaneously by a bank of 12-bit A/D converters. Further details of the data acquisition system are given in Ref. 36.

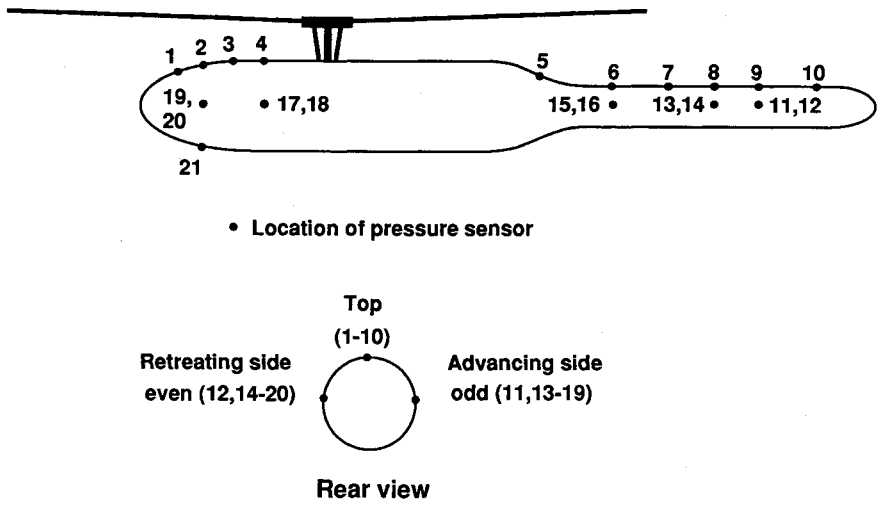

Fig. 2 Locations of pressure sensors.

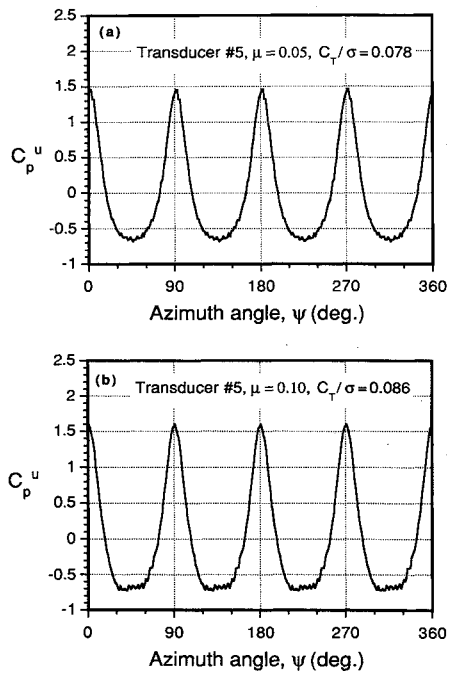

Fig. 3 Type-1 interaction: blade passage effect, unsteady pressure responses directly under the rotor.

Primary data consisted of measurements of the unsteady pressure loads from each sensor for various combinations of advance ratio μ, rotor thrust loading coefficient C_T/σ, and TPP angle α_{TPP}. Time histories of all the sensor responses were logged over 10 rotor revolutions, with a sampling resolution of 1.4 deg of rotor azimuth (256/rev). This was a sufficiently high sampling frequency to resolve unsteady pressure fluctuations over the useful frequency range of the sensor. The data were filtered to remove fluctuations above 4 kHz. The data acquisition system was triggered by 1/rev and 256/rev pulses initiated from an encoder on the rotor shaft.

Flow Visualization

To complement the unsteady pressure measurements, flow visualization of the wake/body interaction process was conducted using wide-field shadowgraphy. The basis of the shadowgraph technique for rotor wake visualization is discussed by Norman and Light[37] and Light et al.[38] Components of the system include a still or a video camera, a short duration high-intensity point-source strobe, and a retroreflective screen. The high-density gradients associated with the tip vortices produce changes in the refractive index of the air. As the strobe light passes through the rotor wake, shadows of the wake vortices are cast on the screen. The camera is focused on the screen and the resulting image captures thin, dark traces identifying the location of the tip vortices. The technique is straightforward and is well suited to rotor wake studies as well as wake/body interactions, yet only the tip vortex is visualized.

Results and Discussion

Unless otherwise noted, the unsteady pressure data presented in this paper are discrete-time histories measured at a TPP angle of attack of -6 deg (a forward tilt of 6 deg). The data are presented as an ensemble average over 10 rotor revolutions. Since the rotor had four blades, the unsteady pressures were periodic at a frequency of 4/rev and were further ensemble averaged over 90 deg of azimuth. It was found that because of the high repeatability and the good signal-to-noise ratio of the data, an average of 10 rotor revolutions (40 events) were sufficient for analysis. For completeness, the event averaged data are shown over a full 360 deg of azimuth.

The time scale was based on the blade azimuth angle; time zero was measured as the ¼-chord of a blade passed over the centerline of the rear body. All of the unsteady pressure data presented in this paper represent the unsteady fluctuations (the AC component) about the mean value of pressure. In addition, the pressures are nondimensionalized using $0.5\rho\Omega^2R^2$ instead of the conventional freestream dynamic pressure. This convention is consistent with the data presented in Ref. 17 and is generally considered a more convenient definition for rotor/body interactional work since the pressure coefficient is independent of the freestream speed and, therefore, gives a more representative measure of the magnitude of the interactional effects at low advance ratios.

Approximately 200 runs were made, which consisted of systematic variations of rotor thrust, TPP angle, and advance ratio. In the present work, the maximum rotor loading coefficient C_T/σ was about 0.09, and the maximum advance ratio was 0.15.

Blade Passage Effects—Type-1 Interactions

Blade passage effects have been measured and reported previously in the literature by Bramwell[26] and later by Brand,[24] although not over the range of thrusts and body positions necessary for full validation of any theory.

The unsteady pressure response measured at location 5 directly under the rotor is shown in Figs. 3 for advance ratios of 0.05 and 0.1 and at a nominal C_T/σ of 0.08. It shows that large 4/rev pulses are produced, which also occur in-phase with the blade passage over the body. This type of signature was found to be relatively independent of advance ratio and appeared to

be mainly associated with the local loading on the rotor itself. In other words, the main features of this type of signature were not coupled to the rotor wake vortex strengths or wake geometry. Therefore, it is conveniently called a blade passage effect. This is called a type-1 interaction in the present work.

This supposition of a pure blade passage effect can be confirmed from a simple potential flow analysis of an infinite series of two-dimensional vortices moving at velocity $\bar{y}\Omega R$ ($\bar{y}=y/R$) at a distance h above a one-dimensional surface. A simple model such as this was first discussed by Bramwell,[26] with later extensions by Lorber and Egolf.[30] A further extension of this simple model using a three-dimensional vortex line has recently been explored by Crouse et al.[33]

The vortex represents the bound circulation at some point on the blade at a distance y from the hub center. The surface, representing the body, is made a streamline to the flow by using an image vortex system. If the circulation along the blade is assumed uniform (a reasonable assumption for a twisted rotor in hover), then the circulation Γ can be related to the blade loading using the expression

$$\Gamma = k\Omega Rc(C_T/\sigma) \tag{1}$$

where k is a constant. It can be shown exactly that $k=2$ for a rotor with constant circulation in hover.[39] With these assumptions, along with Kelvin's equation for the velocity potential, i.e.,

$$\frac{\partial\phi}{\partial t} + \frac{|V|^2}{2} + \frac{p}{\rho} = \text{const} \tag{2}$$

it can be shown that the pressure coefficient at some point x on the surface is given as a function of blade azimuth ψ by the expression

$$C_p^u(\psi) = -100\kappa^2\left[\frac{h/R}{(x/R-\bar{y}\psi)^2+(h/R)^2}\right]^2 + 200\kappa\left[\frac{h/R\bar{y}}{(x/R-\bar{y}\psi)^2+(h/R)^2}\right] \tag{3}$$

where

$$\kappa = \frac{k(c/R)(C_T/\sigma)}{\pi} \tag{4}$$

The first term in Eq. (3) is the quasisteady contribution, and the second term is the unsteady contribution, i.e., the $\partial\phi/\partial t$ term. The result is shown in Fig. 4, where the theoretical pressure signature is in excellent quantitative agreement with the test data of Figs. 3. The unsteady term is clearly much more significant than the quasisteady term, and this illustrates the necessity of retaining the time-dependent velocity potential terms in any rotor/body interaction model. The importance of the unsteady terms has been noticed and discussed by other workers,[26,30] although only limited and incomplete validation has previously been conducted with experimental measurements of the phenomenon.

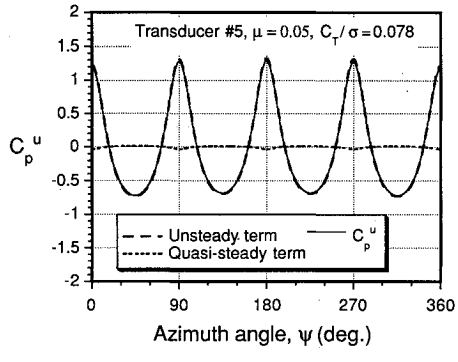

Fig. 4 Blade passage signature as predicted by potential flow theory.

The significance of the unsteady terms is further explored here by comparing with other experimental data measured on the fuselage directly under the rotor disk. According to the simple model described by Eq. (3), the approximate magnitude of the unsteady pressures on the body due to blade passage should be 1) proportional to the rotor disk loading C_T/σ (or more strictly, to the local blade loading), 2) inversely proportional to the distance of the rotor blades above the measurement point, and 3) proportional to the speed of the bound vortex above the point. Thus, it can be immediately concluded that the unsteady loads induced due to blade passage effects will become much more pronounced on rotorcraft with high disk loadings, higher tip speeds, and smaller rotor/fuselage spacings.

Figure 5a presents a comparison of the peak-to-peak values of the unsteady pressure at two points directly below the rotor as a function of rotor thrust at $\mu=0.15$. It can be seen that the agreement of theory and experiment in Fig. 5a is good. Despite some nonlinear behavior in the test data, which is probably due to three-dimensional effects and nonuniform variation in circulation along the blade as advance ratio increases, this simple model clearly confirms the validity of a more general potential flow theory in predicting the unsteady pressures on the body due to blade passage effects.

The blade passage effect was also found to be largely independent of advance ratio, although the distribution of loading on each individual blade becomes increasingly different with increasing advance ratio. Figure 5b shows the peak-to-peak values of the unsteady pressure (at the same locations as Fig. 5a) vs advance ratio at two different values of rotor thrust. This figure shows that the unsteady pressures associated with blade passage effects remain nominally constant at a given point on the body for increasing advance ratio. This is to be expected because any changes in either advance ratio or TPP angle will only slightly affect longitudinal variation of lift over the rotor disk, i.e., the distribution of circulation on the rotor blades as they pass above the body. This is not so for the advancing and retreating blades, although because of their increased relative distance from the measurement point, the influence on the body pressures is small. In general, changes in

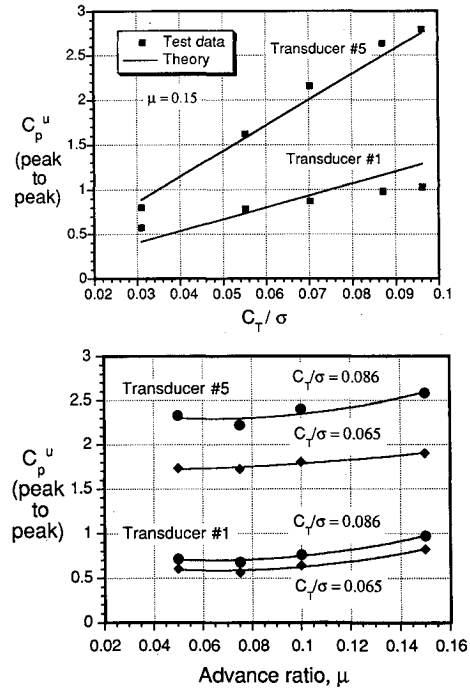

Fig. 5 Peak-to-peak values of the unsteady pressures directly under the rotor.

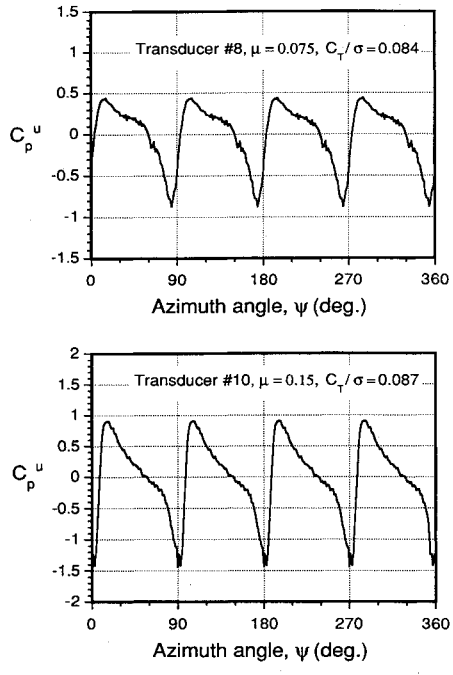

Fig. 6 Type-2 interaction: close wake/body interaction, unsteady pressure responses on the tail boom.

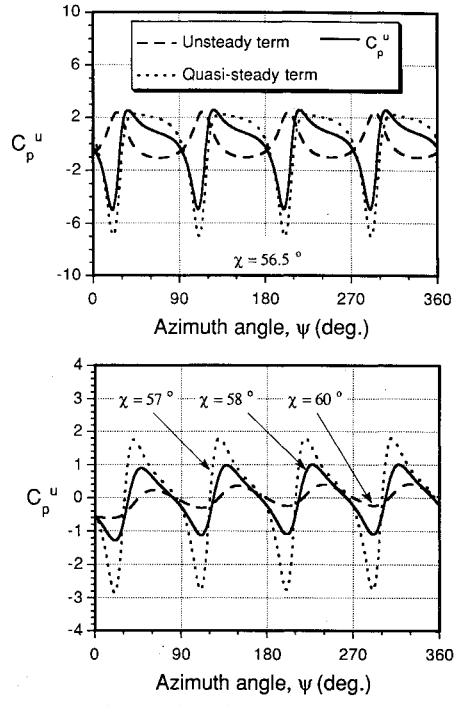

Fig. 7 Close wake interaction signature as predicted by potential flow theory.

advance ratio in the lower range will not severely affect the total circulation strength on the rotor while the total thrust loading coefficient on the rotor is maintained, as confirmed by Fig. 5b.

Close Wake/Body Interactions—Type-2 Interactions

Figures 6 illustrate a second type of pressure signature frequently observed in this experiment, which is different in character to the blade passage effects shown in Figs. 3. It can be seen that both the signatures in Figs. 6 are characterized by a sawtooth-type waveform, which is predominantly 4/rev but with many higher harmonics. In contrast to the blade passage effects that were confined to the regions of the body directly below the rotor,[33] this second type of signature was found to occur at different points on the rear of the body under a variety of combinations of thrust and advance ratio. In fact, it was possible to track this signature to different points on the body through variations in rotor thrust and advance ratio; in other words, by systematically moving the location of the rotor wake relative to the body.

Further recent study using the shadowgraphic flow visualization technique has led to the conclusion that the signatures shown in Figs. 6 are closely associated with the proximity, trajectory, and convection velocity of the trailed wake vortex filaments relative to the body. This has also been verified from a study of the induced velocity field and wake boundaries, as reported by Leishman and Bi.[40] For the data shown in Figs. 6, the wake filaments were found to be close to the pressure sensor, but were not directly impinging in its locality. In other words, the wake vortices were convected downstream a small distance above the body surface. Thus, these pressure signatures are called close wake interactions, or simply type-2 interactions. This characteristic signature also appears to be present in some data reported in Ref. 25, although it is difficult to isolate from the more dominant blade passage effects. It is also interesting that the signatures shown in Figs. 6 are qualitatively similar to the time history of the inflow velocity near a rotor as measured using a laser velocimeter, for example, see Ref. 41.

Of course, the actual pressure signature induced on the body by the wake depends not only on the relative speed, direction, and proximity between the wake filament and the measurement location, but also on the strength of the rotor wake vortices, i.e., rotor thrust. This situation also can be examined, albeit approximately, by using potential flow theory that is similar to that conducted earlier for the blade passage effects. Such a theory has been proposed by Lorber and Egolf,[30] but without validation against experimental data.

The simplest model consists of an infinite series of free vortices convecting at velocity $\mu\Omega R$ at a skew angle χ relative to the vertical. The purpose of using a simple model is to help clarify the type of signature induced by vortices passing over a fixed location on the body. Again, an image system is included to satisfy the condition of flow tangency on the surface. According to Helmholtz's theorem, strength of the free tip vortex must be related to the circulation on the blade (i.e., rotor thrust), and it can be shown that the unsteady pressure coefficient on the body due to the convecting wake at a skew angle χ is given as a function of ψ by the expression

$$C_p^u(\psi) = -100\kappa^2\left\{\frac{b/R - \mu\psi\tan(\chi)}{(x/R-\mu\psi)^2+\left[b/R-\mu\psi\tan(\chi)\right]^2}\right\}^2 - 200\mu\kappa\left\{\frac{x/R\tan(\chi)-b/R}{(x/R-\mu\psi)^2+\left[b/R-\mu\psi\tan(\chi)\right]^2}\right\} \quad (5)$$

where, again, κ is given by Eq. (4), and k is assumed to be 2.0.

The first term in Eq. (5) is the quasisteady contribution and the second term is the unsteady effect, with the results being shown in Figs. 7. It can be seen that the predicted pressure signature is in excellent qualitative agreement with the test data of Figs. 6. This level of correlation essentially confirms that this second type of pressure signature was induced by a close wake vortex/body interaction. It should be noted, however, that compared to the blade passage effect shown in Fig. 4, in this latter case both the quasisteady term and the unsteady term are of extreme importance in determining the net pressure signature, another result concluded in Ref. 30 but without experimental verification.

The large sensitivity of the unsteady pressure signature to hypothetical changes in the wake skew angle, i.e., the height of the convecting wake vortices over the body location, is also shown in Figs. 7. At the lower wake skew angle ($\chi = 57$ deg), the sawtooth type of pressure signature induced on the body is clearly due to a type-2 interaction (i.e., close wake interaction). However, when the wake skew angle is just slightly higher

($\chi = 60$ deg), the induced pressure signature becomes more benign. In fact, the pressure signature at higher skew angles gradually becomes more like a blade passage effect since the wake makes an increasingly parallel angle with the body surface with increasing μ at a constant C_T/σ.

Although these calculations represent hypothetical changes in skew angle, remember that, in reality, the wake skew angle is a more complex function of the rotor thrust, the distribution of loading over the rotor disk, the advance ratio, self-induced wake distortion, as well as the amount of local wake distortion near the fuselage. This latter effect usually increases the wake skew angle at the rear of the rotor and decreases the skew angle at the front.[38,42] Therefore, it can be concluded that although an unsteady potential flow model is sufficient to predict the close wake/body interactions when the vortex strengths and locations are prescribed, the high sensitivity of the body pressures to changes in wake location shown in Figs. 7 means that accurate prediction of the rotor wake geometry is really the key to successful prediction of rotor wake/airframe interactional airloads. Since it is very difficult to predict (or measure) the wake geometry to high accuracy, the accurate prediction of type-2 interaction signatures at specific points on the airframe may be very difficult or impossible.

Wake/Body Impingement—Type-3 Interactions

A third characteristic type of pressure signature measured in the present experiments is shown in Fig. 8. This signature appeared to result from direct wake impingement near the measurement point, a fact confirmed by the shadowgraphic flow visualization experiments. A typical shadowgraph result is shown in Fig. 9, where the tip vortex filaments appear as thin, dark spirals. The cross hairs on the screen are reference points used to help quantify the wake geometry and body sensor locations. Near the body surface, it can be seen that the local wake skew angle progressively increases as the filaments asymptotically approach the body surface. The wake filaments also appear to undergo significant local distortion (both laterally and longitudinally) and convect some distance along the surface of the body before viscous diffusion causes the visibility of the vortices to diminish. The physics of such complicated wake/body distortions are discussed by Quackenbush and Bliss.[43]

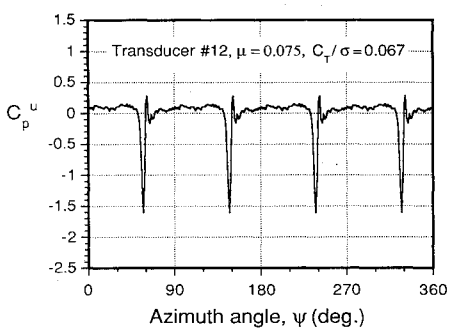

Fig. 8 Type-3 interaction: wake/body impingement.

Fig. 9 Shadowgraph photo of wake near rear fuselage.

As with type-2 signatures, type-3 wake/body impingement signatures could be relocated to other parts of the body by changes in rotor thrust or advance ratio. Although these pressure responses were still primarily 4/rev, in contrast to the blade passage interactions (type 1) and close wake interactions (type 2), this third type of pressure signature is much more of a transient nature. It is certainly interesting that these signatures look similar to those obtained during a blade vortex interaction; see, for example, Ref. 44.

It should be pointed out that type-3 pressure signatures are not easily captured since the spatial resolution of pressure sensors on the body is not great. Type-3 interactions only occur when the trailed wake filaments from the rotor blade tips impinge very near the measurement point. In practice, this is not easy to achieve since the trailed wake geometry is a complicated function of the rotor thrust and advance ratio and the local distortion of the wake as it approaches the body. Progressive transitions from type-3 to type-2 interactions (or vice versa) were found during judicious adjustments of the advance ratio and/or rotor thrust, therefore adjusting the position of the rotor wake vortices (and degree of wake distortion) relative to the body.

Postwake Impingement—Type-4 Interactions

A fourth possible type of pressure characteristic signature is shown in Fig. 10, which generally appeared to occur just downstream of a wake impingement point on the body. This is referred to as a postimpingement or type-4 interaction. This type of signature was referred to as a direct wake impingement interaction in Ref. 36. However, as a result of shadowgraphic flow visualization of the wake vortex/body interaction process,[45] the present study has shown that wake impingement actually occurred just upstream of the measurement point under the test conditions shown in Fig. 10.

Comparing this type-4 signature with types 2 and 3, shown by Figs. 3 and 6, respectively, it can be seen that this signature contains certain features common to both types 2 and 3. The

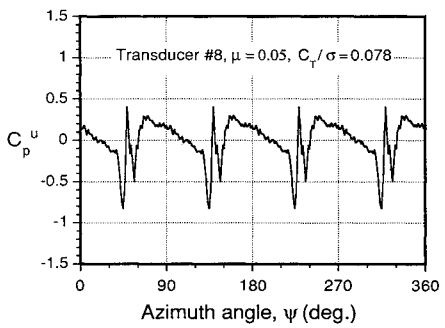

Fig. 10 Type-4 interaction: postwake impingement.

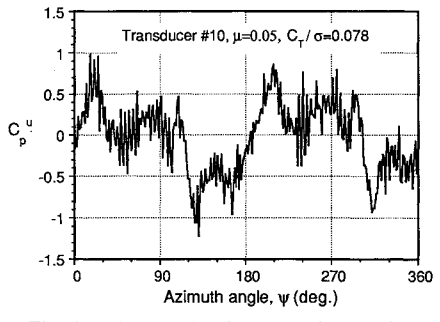

Fig. 11 Far postimpingement interaction.

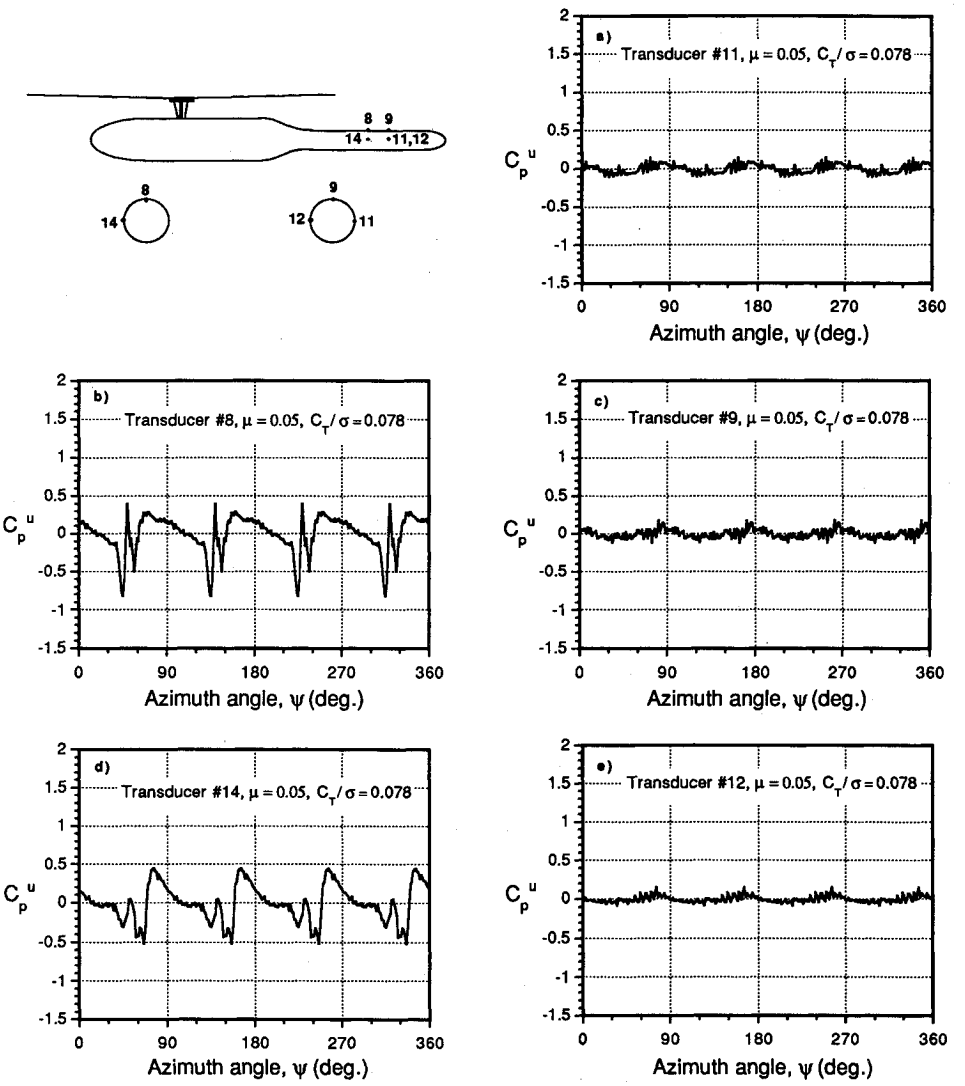

Fig. 12 Unsteady pressure responses on the top and sides of the rear fuselage at $\mu = 0.05$.

basic sawtooth pattern is present, along with a transient loading, but with several additional spikes. The amplitude of the dominant spike was also attenuated relative to the type-3 interactions. This is a very complicated signature and may be very difficult to predict even when the rotor wake geometry is accurately prescribed, as discussed in Ref. 33. Prediction of type-4 interactions will involve a more thorough understanding of the wake vortex filaments during, and after, the wake interaction with the body. Such effects have been investigated both here and elsewhere, but are still poorly understood at present.

Our observations show that type-4 pressure signatures can be further classified into two groups. One can be called a near postimpingement interaction, and the other a far postimpingement interaction. The near postimpingement signatures occur immediately downstream of the location where the rotor wake filament impacts or at least comes very close to the body surface. The far postimpingement occurs some farther distance downstream. Figure 11 shows a typical signature for the far postimpingement interaction, whereas Fig. 10 shows the near postimpingement interaction. Figure 11 was constructed using unaveraged data (the data from the fifth rotor revolution). It can be seen that the far postimpingement interaction signature contains many higher frequency fluctuations due to higher frequency flow fluctuations. The unsteadiness arises because part of the wake vortex that is very close to the body becomes unsteady as it undergoes a complicated stretching and diffusion process. This has been observed with the shadowgraph method and recorded on video tape.[45] The other main difference between Figs. 10 and 11 is their ensemble averaging features, which will be discussed later.

Details of Wake/Body Impingement

It has been shown that type-1 interactions are somewhat straightforward to predict, whereas type-2 interactions only can be predicted if both the rotor thrust (wake vortex strengths) and the wake geometry are accurately predicted. Current wake prediction methodologies do not yet seem to have the level of accuracy required for this type of calculation, particularly since the local distortion of the wake due to the body must be accounted for. This latter effect, that is, the behavior of the rotor wake filaments when they approach, distort, and impact the body surface, seems to be one major concern in the prediction of the rotor wake/body aerodynamic interactions.[44] Thus, one of the efforts in the present work was to further explore this phenomenon.

Some work has been done in experimental fluid dynamics that shows the amazing complexity of the interactions between vortices and solid surfaces, though this work has not specifically addressed rotor/body interactions. Lim,[42] Atias and Weihs,[46] Doligalski and Walker,[47] and Walker et al.[48] are notable examples. These workers showed that the interactions were very complicated, involving a complex balance of inertia, pressure, and viscous forces. Another notable study by Simons et al.[49] showed the wake behavior around a pylon. The convection and breakdown of trailing vortex from a rotor blade was

examined, and it was noted that the tip vortex from the blade deformed and appeared to wrap around the nose of the rotor supporting pylon. Laser sheet visualization of rotor wake by Georgia Institute of Technology workers[19] has also helped clarify the trajectories of rotor wake vortices as they approach a solid body.

The shadowgraphic observations of the rotor wake for the present rotor/body configuration have provided considerably more guidance in establishing a qualitative understanding of the wake behavior as it approaches the body. The quantitative measurements of the unsteady body pressures have helped to clarify further some of the possible mechanisms.

Figures 12–15 show the pressure responses measured at two stations on the top and sides of the body for advance ratios of 0.05, 0.075, 0.10, and 0.15, respectively, and at a nominal rotor loading coefficient of 0.08. The results from sensor 13 are missing from these plots due to a malfunctioning A/D converter. For the lowest advance ratio of 0.05, as shown in Figs. 12, it appeared that wake impingement on the body first took place very close to sensor location 8, since Fig. 12b shows that pressure response measured at this point was of a type-4 interaction. The somewhat benign responses from sensors 9, 11, and 12 at the body station just downstream initially suggests that the wake may be locally cut, or even catastrophically destroyed, by the interaction with the body. This is only partially confirmed by the shadowgraph results since the visibility of the wake quickly diminishes when viscous effects diffuse the wake vortex structures.

When the advance ratio was increased to 0.075, as shown in Figs. 13, the responses from the various sensors take on a slightly different character. Since the mean skew angle of the wake was slightly greater for this advance ratio (based on momentum theory, $\chi = 59$ deg compared with $\chi = 42$ deg at $\mu = 0.05$), the wake impingement point occurred farther aft on the body. The signatures from sensors 9, 11, and 12 at the aft body station all resembled a type-4 interaction, showing that the wake had impinged the body near this station, but had likely been pushed around the sides of the body during the impingement.

At the upstream station, sensor 8 showed a classic, although slightly attenuated, type-2 interaction, indicating that the convected wake was just above the surface at this location. Sensor 14 also gives an interesting response, which is relatively similar to the type-2 interactions, but is also sufficiently different that it could even be classified as a separate type. However, this signature is still due to a close wake interaction, although because it occurs on the side of the body, it has this waveform mainly because of surface curvature effects, i.e., because of the geometric relationship between the induced velocity field on the top of the body vs that on the sides. A theoretical discussion of the effects of surface curvature is beyond the scope of the present paper. This type of signature can only be predicted by using a full three-dimensional model for the body.

In Figs. 14, the results for an advance ratio of 0.10 are shown. It appeared that for this advance ratio the wake skew angle was now sufficiently high that the wake vortices impinged near the tail of the body downstream of location 9. Sensor 9 showed a classic type-2 interaction, indicating the wake passed above the body at this point. On the sides of the body, at locations 11 and 12, similar signatures to that shown

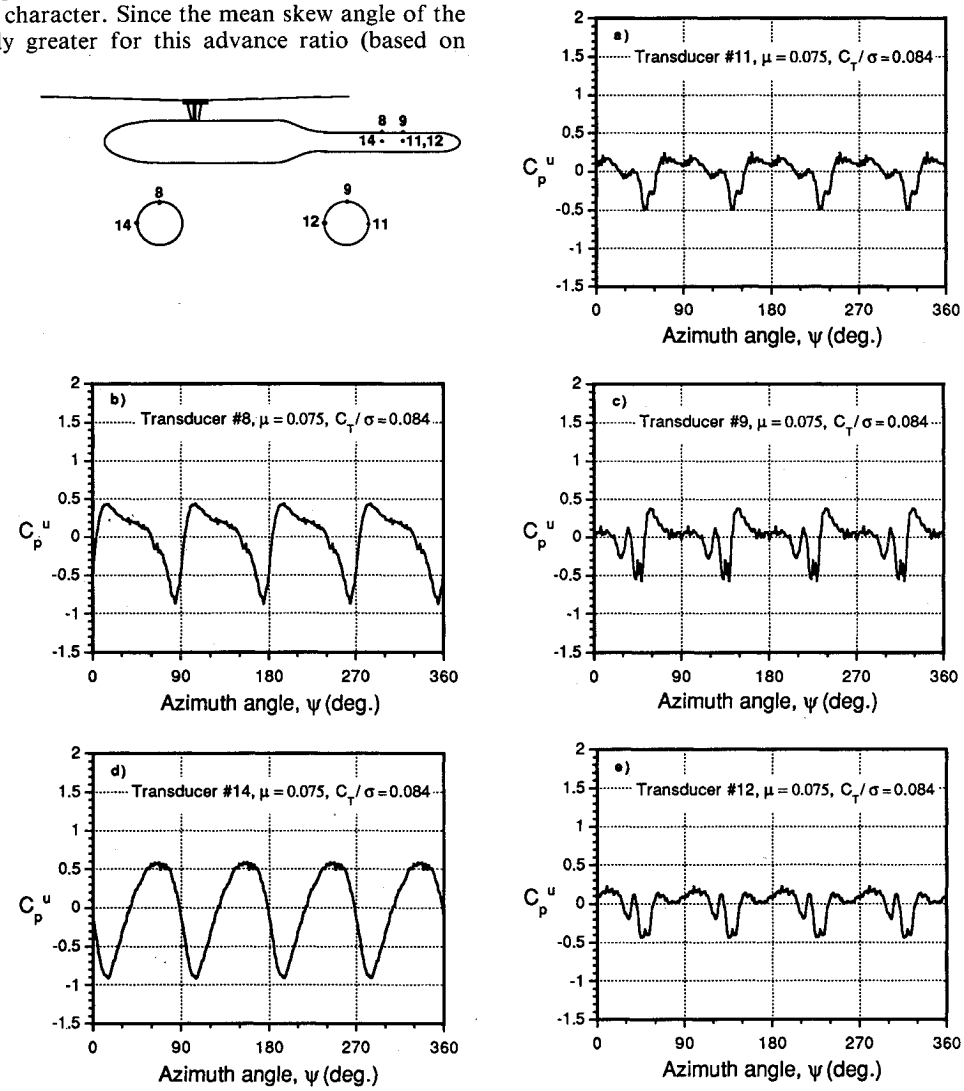

Fig. 13 Unsteady pressure responses on the top and sides of the rear fuselage at $\mu = 0.075$.

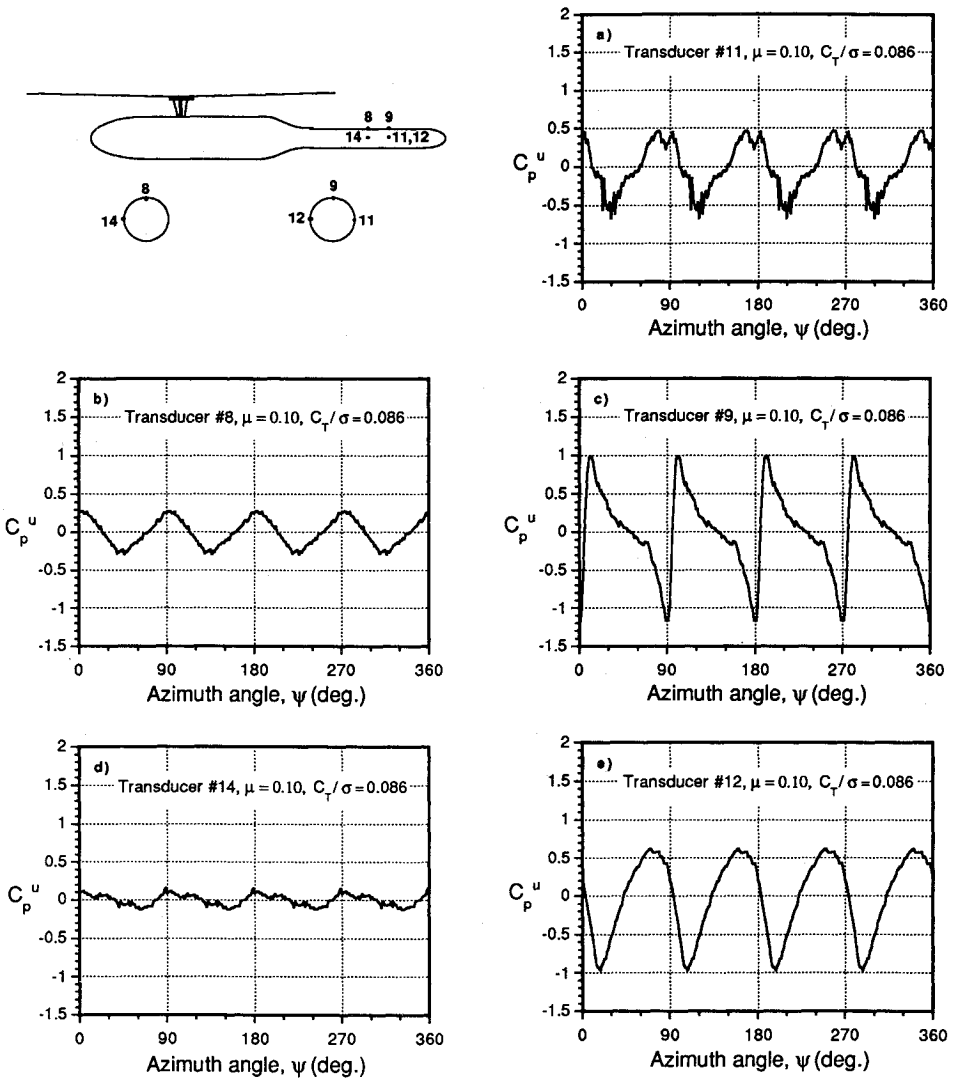

Fig. 14 Unsteady pressure responses on the top and sides of the rear fuselage at $\mu = 0.10$.

in Fig. 13d were produced. This essentially confirms that these types of signatures are still representative of close wake vortex interactions with the body, but again differ from Fig. 13c mainly because of the surface curvature. It also should be noted that the responses from sensors 11 and 12 are just slightly out of phase, indicating that the vortex filament arrives slightly later at the left side (retreating side) of the body. The additional higher frequency fluctuations at location 11 also indicate that the wake vortices are closer to the right side of the fuselage. This is to be expected since it is well known that a rotor in forward flight induces a lateral variation in downwash that is biased to the advancing side of the disk,[50] and so the axial displacements of the wake filaments are greater on this side. At the upstream body station, sensors 8 and 14 produce relatively benign outputs since the vortex filaments are farther above the surface compared with the previous advance ratio of 0.075.

The results for the highest advance ratio of 0.15 are shown in Figs. 15. For this test condition, all of the sensors showed very similar outputs since the mean skew angle of the wake was quite high ($\chi \approx 80$ deg), and the wake vortices were convected relatively far above the main part of the fuselage. It was interesting, however, that even though the wake was farther away from the fuselage at this advance ratio, the magnitude of the induced pressure signature at location 14 was a little larger than that at the lower advance ratio of 0.10 shown in Fig. 15d. This is because the unsteady pressure induced by the wake is actually a function of both the proximity to the wake vortices to the body surface as well as the relative convection speed. For the higher advance ratio, the reduction in pressure due to the higher wake skew angle is actually negated by the increased convection speed of the rotor wake vortices. Thus, though the wake is farther away from the body and, based on steady flow concepts, would be expected to have minimal effects on the body pressures, these results indicate that unsteady pressure effects induced on the body by the trailed wake filaments at high advance ratios could be very important on rotorcraft, in general.

Comparison of Averaged and Unaveraged Data

The proper selection of a representative time series of pressure measurements is essential to accurately discern, and ultimately understand, the nature of the interaction phenomena. It is well known that, for an isolated rotor system, the flowfield environment is periodic. The fundamental frequencies are multiple integers of the main rotor rotational frequency. Thus, it is a normal procedure to select information over any one period (one rotor revolution or one blade passage) to be representative of the whole unsteady event. More often, the unsteady data are acquired over several periods. The representative unsteady signature for one period is then obtained by ensemble averaging the data over these periods to improve the signal-to-noise ratio.

In the present study, it has been found that the unsteady pressures on the body contain mostly periodic components at multiples of the rotor frequency, although some locations also

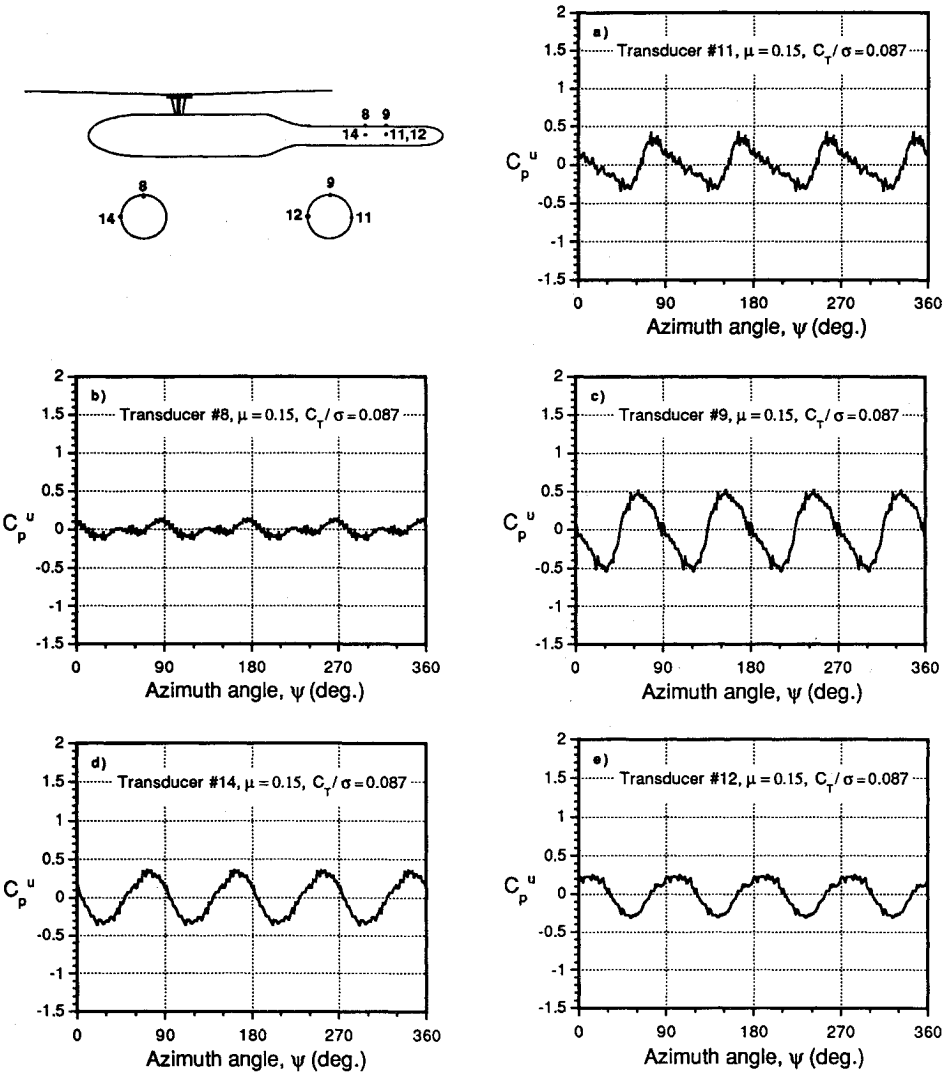

Fig. 15 Unsteady pressure responses on the top and sides of the rear fuselage at $\mu = 0.15$.

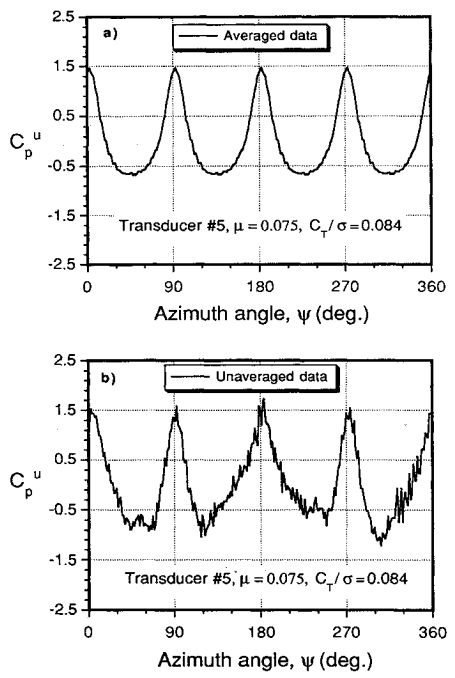

Fig. 16 Comparison of averaged and unaveraged unsteady pressure responses for type-1 interaction.

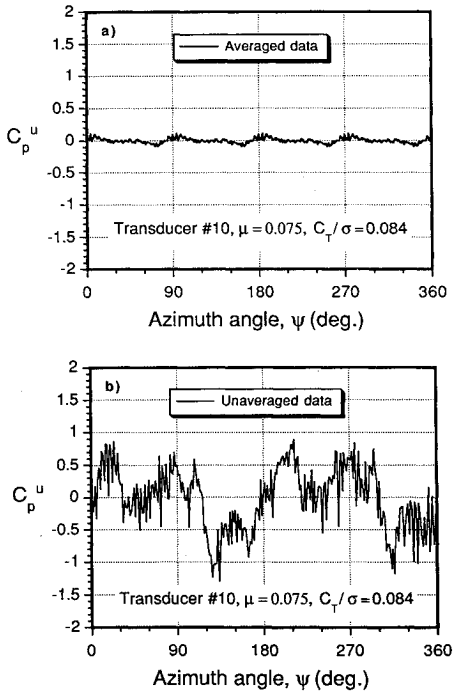

Fig. 17 Comparison of averaged and unaveraged unsteady pressure responses for type-4 interaction.

appear to have significant nonperiodic components. At least, the so-called nonperiodic components do not appear to be periodic relative to the rotor frequency. Therefore, some additional attention was paid to selecting representative data during the unsteady airloads measurements. Two types of representative data were generally selected, namely, event-averaged data or unaveraged data. The event-averaged data for one rotor revolution is the ensemble average of 40 events over 10 rotor revolutions. The discrete-time histories of the unsteady pressure from an individual rotor revolution is called unaveraged data. In this paper, representative unaveraged data are taken from the fifth rotor revolution after the start of the data acquisition process.

Figures 16 show a typical comparison of the averaged data and unaveraged data for a type-1 (blade passage) interaction. It can be seen that the unaveraged data are quite representative of a typical event since the averaged data retains all of the salient features of the ensemble average. On the other hand, Figs. 17 show that there is a considerable difference between the averaged data and the unaveraged data. For the averaged data, the signature is quite benign and may suggest to the analyst that the interactional effects between the rotor wake and the body are negligible. The unaveraged data is more random, although repeated examination of the time histories over many rotor revolutions still showed a clear characteristic structure and periodicity, even though this periodicity was not at the rotor frequency.

Further study has shown that the reason for this behavior was related phase differences in the signal during each rotor revolution, though the main characteristics of the signal were present during every rotor revolution. Thus, because of the phase shift, the signal was effectively canceled when averaging the data at the rotor frequency. The physical reason for this problem remains as yet unknown, although it may be related to the fact that lower frequency phenomena, such as vortex shedding from the body, may be present in the region downstream of the rotor wake boundary. Also, after the wake impingement on the body, the remaining wake becomes very much more unsteady as it is convected along the body surface.[45] Anyhow, it appears that caution should be exercised when averaging data over several periods when studying rotor/body aerodynamic interactions, especially in regions where separated flows or wake vortex/surface impingement also may be present. In such cases, averaging the measured data could be misleading when attempting to understand the underlying physics of the interaction process.

Conclusions

This paper has summarized the characteristics of unsteady surface pressures induced on a body in the presence of a rotor. The measurements have been conducted with the objective of more completely isolating contributions to the body airloads made by different interaction mechanisms and assessing their significance in the whole framework of rotor/body aerodynamic interactions.

Four basic types of rotor/body interactions were discerned; two types were verified by unsteady potential flow models. Studies of the wake/body interaction were also made using shadowgraphic flow visualization. These observations were used to explain further the possible physics of a rotor wake vortex filament impinging on the body.

The results from this study have contributed to an improved understanding of the possible mechanisms, but have also demonstrated that the interactional phenomena between a rotor and a body are very complicated and, as of yet, are not completely understood. Further measurements must be conducted on the wake impingement problem.

The following conclusions have been drawn from the present study.

1) Characteristic pressure signatures on the body were identified and attributed to four types of interactions: 1) blade passage effect, 2) close wake vortex/body interaction, 3) wake impingement on the body, and 4) postwake impingement.

2) Good correlations were obtained between test data and potential models for type-1 and type-2 interactions. The close wake interactions (type 2) could only be predicted quantitatively if the rotor wake vortex positions were accurately prescribed. In the predictions, the unsteady potential terms must be retained in the analysis to give sensible predictions of the pressure signatures.

3) Variations in the rotor thrust and advance ratio were found to have very significant effects on the unsteady pressures measured on the body. Blade passage effects were a function mainly of the rotor thrust; however, wake vortex induced effects were a more complicated function of both thrust and advance ratio. An extremely high sensitivity of the induced pressure loads due to wake skew angle was noted. Such sensitivities raise doubts about the ability of existing rotor wake methodologies to predict the body pressure signatures, particularly when body induced wake distortion must be accounted for.

4) At intermediate advance ratios, the trailed wake passed relatively far above the body and had relatively small effects on the body pressures. Yet, as the advance ratio was increased further, the unsteady pressures on the body became significant again due to the higher convection velocity of the trailed wake filaments.

5) Wake impingement on the body did not necessarily produce the most significant airloads. To the contrary, blade passage effects and close wake interactions with the body were found to produce more significant unsteady pressure loadings.

6) Special attention should be paid to the selection of representative data for a whole unsteady event, particularly if there is reason to suspect that separated flows may be involved. Because of the overall complexity of the interaction phenomena, the characteristic pressure loads may be misinterpreted using cycle-averaged or event-averaged data, and some caution should be exercised.

Acknowledgments

Most of this work was supported by the U.S. Army Research Office under Contract DAAL-03-88-C002. Thomas Doligalski was the technical monitor. The shadowgraph work was partially supported by the Rotorcraft Aeromechanics Branch at NASA Ames Research Center under NASA Grant NAG2-607, the technical monitor was Jeffrey S. Light. The authors wish to thank Rotorcraft Center research engineer Dhananjay Samak for his help in conducting the experiments and Jewel Barlow for his cooperation in accommodating the tests in the Glenn L. Martin wind tunnel.

References

[1]Larin, A. V., "Vortex Wake Behind a Helicopter," *Aviatsiya i Kosmonavtika,* No. 3, 1973, pp. 32-33.

[2]Main, B. J., and Mussi, F., "EH101—Status Report," *Proceedings of the 16th European Rotorcraft Forum,* Glasgow, Scotland, Sept. 1990.

[3]Prouty, R. W., "Development of the Empennage Configuration of YAH-64 Advance Attack Helicopter," USAAVRADCOM-TR-82-D-22, Feb. 1983; also, Prouty, R. W., Amer, K. B., "The YAH-64 Empennage and Tail Rotor—A Technical History," 38th Annual Forum of the American Helicopter Society, Anaheim, CA, May 1982.

[4]Landgrebe, A. J., Moffitt, R. C., and Clark, D. R., "Aerodynamic Technology for Advanced Rotorcraft," *Journal of the American Helicopter Society,* Vol. 22, No. 2, 1977, pp. 21-27; Vol. 22, No. 3, 1977, pp. 2-9.

[5]Berry, J. D., and Althoff, S. L., "Inflow Velocity Perturbations Due to Fuselage Effects in the Presence of a Fully Interactive Wake," *Proceedings of the 46th Annual Forum of the American Helicopter Society,* Washington, DC, May 1990.

[6]Fail, R. A., and Eyre, R. C., "Loss of Static Thrust Due to a Fixed Surface Under a Helicopter Rotor," British Royal Aeronautical Establishment, TN Aero 2008, 1949.

[7]Makofski, R. A., and Menkick, G. F., "Investigation of Vertical Drag—Periodic Airloads Acting on Flat Panels in a Rotor Slipstream," NACA TN 3900, 1956.

[8]Payne, P. R., *Helicopter Dynamics and Aerodynamics,* Macmillan, New York, 1959.

[9]Sheridan, P. F., and Smith, R. P., "Interactional Aerodynamics—A New Challenge to Helicopter Technology," *Proceedings of the 35th Annual Forum of the American Helicopter Society,* Preprint No. 79-59, Washington, DC, May 1979.

[10]Wilson, J. C., and Mineck, R. E., "Wind-Tunnel Investigation of Helicopter Rotor Wake Effects on Three Helicopter Fuselage Models," NASA TM X-3185, March 1975.

[11]Betzina, M. D., and Shinoda, P., "Aerodynamic Interactions Between a 1/6-Scale Helicopter Rotor and a Body of Revolution," NASA TM X-84247, June 1982.

[12]Smith, C. A., and Betzina, M. D., "Aerodynamic Loads Induced by a Rotor on a Body of Revolution," *Journal of the American Helicopter Society,* Vol. 31, No. 1, 1986, pp. 29–36.

[13]Komerath, N. M., McMahon, H. M., and Hubbard, J. E., "Aerodynamic Interactions Between a Rotor and Airframe in Forward Flight," AIAA Paper 85-1606, 1985.

[14]McMahon, H. M., Komerath, N. M., and Hubbard, J. E., "Studies of Rotor-Airframe Interactions in Forward Flight," AIAA Paper 85-5015, Oct. 1985.

[15]Brand, A. G., Komerath, N. M., and McMahon, H. M., "Results from a Laser Sheet Visualization of a Periodic Rotor Wake," AIAA Paper 88-0192, Jan. 1988.

[16]Liou, S. G., Komerath, N. M., and McMahon, H. M., "The Velocity Field of a Lifting Rotor in Low-Speed Forward Flight," AIAA Paper 88-0666, AIAA 26th Aerospace Sciences Meeting, Reno, NV, Jan. 1988.

[17]Liou, S. G., Komerath, N. M., and McMahon, H. M., "Velocity Measurement of Airframe Effects on a Rotor in Low-Speed Forward Flight," *Journal of Aircraft,* Vol. 26, No. 4, 1989, pp. 340–348.

[18]Brand, A. G., McMahon, H. M., and Komerath, N. M., "Surface Pressure Measurements on a Body Subject to Vortex-Wake Interaction," *AIAA Journal,* Vol. 27, No. 5, 1989, pp. 569–574.

[19]Liou, S. G., Komerath, N. M., and McMahon, H. M., "Measurement of Transient Vortex-Surface Interaction Phenomena," *AIAA Journal,* Vol. 28, No. 4, 1989, pp. 975–981.

[20]Mavris, D. N., Komerath, N. M., and McMahon, H. M., "Prediction of Rotor/Airframe Aerodynamic Interactions," *Journal of the American Helicopter Society,* Vol. 34, No. 4, 1989, pp. 37–46.

[21]Brand, A. G., McMahon, H. M., and Komerath, N. M., "Correlations of Rotor/Wake-Airframe Interactions with Flow Visualization Data," *Proceedings of the 46th Annual Forum of the American Helicopter Society,* Washington, DC, May 1990.

[22]Liou, S. G., "Velocity Measurements on a Lifting Rotor/Airframe Configuration in Low Speed Forward Flight," Ph.D. Dissertation, Georgia Inst. of Technology, Atlanta, GA, Dec. 1988.

[23]Marvis, D. N., "An Analytical Method for the Prediction of Unsteady Rotor/Airframe Interactions in Forward Flight," Ph.D. Dissertation, Georgia Inst. of Technology, Atlanta, GA, Dec. 1988.

[24]Brand, A. G., "An Experimental Investigation of the Interaction Between a Model Rotor and Airframe in Forward Flight," Ph.D. Dissertation, Georgia Inst. of Technology, Atlanta, GA, March 1989.

[25]Brand, A. G., McMahon, H. M., and Komerath, N. M., "Wind Tunnel Data for a Rotorcraft Airframe Interaction Study," School of Aerospace Engineering, Georgia Inst. of Technology, Atlanta, GA, July 1986.

[26]Bramwell, A. R. S., "A Theory of the Aerodynamic Interference Between a Helicopter Rotor Blade and a Fuselage and Wing in Hovering and Forward Flight," British R&M 3514, June 1965; also, *Journal of Sound and Vibration,* Vol. 3, No. 3, 1966, pp. 355–383.

[27]Clark, D. R., and Maskew, B., "Study for Prediction of Rotor/Wake/Fuselage Interference," NASA CR-177340, March 1985.

[28]Clark, D. R., and Maskew, B., "Calculation of Unsteady Rotor Blade Loads and Blade/Fuselage Interference," *Proceedings of the Second International Conference on Rotorcraft Basic Research,* College Park, MD, Feb. 1988.

[29]Freeman, C. E., "Development and Validation of a Combined Rotor-Fuselage Induced Flow-Field Computational Method," NASA TP-1656, June 1980.

[30]Lorber, P. F., and Egolf, T.A., "An Unsteady Helicopter Rotor-Fuselage Interaction Analysis," NASA CR-4178, Aug. 1988.

[31]Berry, J. D., "Prediction of Time-Dependent Fuselage Pressures in the Wake of a Helicopter Rotor," *Proceedings of the Second International Conference on Rotorcraft Basic Research,* College Park, MD, Feb. 1988.

[32]Rand, O., "The Influence of Interactional Aerodynamics in Rotor/Fuselage Coupled Response," *Proceedings of the Second International Conference on Rotorcraft Basic Research,* College Park, MD, Feb. 1988.

[33]Crouse, G. L., Leishman, J. G., and Bi, N., "Theoretical and Experimental Study of Unsteady Rotor/Body Aerodynamic Interactions," *Proceedings of the 46th Annual Forum of the American Helicopter Society,* Washington, DC, May 1990.

[34]Quackenbush, T. R., and Bliss, D. B., "Free Wake Calculation of Rotor Flow Fields for Interactional Aerodynamics," *Proceedings of the 44th Annual Forum of the American Helicopter Society,* Washington, DC, June 1988.

[35]Leishman, J. G., and Bi, N., "Aerodynamic Interactions Between a Rotor and a Fuselage in Forward Flight," *Journal of the American Helicopter Society,* Vol. 35, No. 3, 1990, pp. 22–31.

[36]Bi, N., and Leishman, J. G., "Experimental Study of Aerodynamic Interactions Between a Rotor and a Fuselage," AIAA Paper 89-2211, AIAA 7th Applied Aerodynamics Conference, Seattle, WA, July 1989; also, *Journal of Aircraft,* Vol. 27, No. 9, 1990, pp. 779–788.

[37]Norman, T. R., and Light, J. S., "Rotor Tip Vortex Geometry Measurements Using the Wide-Field Shadowgraph Technique," *Journal of the American Helicopter Society,* Vol. 32, No. 2, 1987, pp. 40–50.

[38]Light, J. S., Frerkin, A., and Norman, T. R., "Application of the Wide-Field Shadowgraph Technique to Helicopters in Forward Flight," *Proceedings of the 46th Annual Forum of the American Helicopter Society,* Washington, DC, May 1990.

[39]Stepniewski, W. Z., and Keys, C. N., *Rotory-Wing Aerodynamics,* Dover, New York, 1984.

[40]Leishman, J. G., and Bi, N., "Measurements of a Rotor Flowfield and the Effects on a Body in Forward Flight," *Proceedings of the 16th European Rotorcraft Forum,* Glasgow, Scotland, Sept. 1990; also, *Vertica,* Vol. 14, No. 3, 1990, pp. 401–415.

[41]Elliott, J. W., and Susan, L. A., "Inflow Measurement Made with a Laser Velocimeter on a Helicopter Model in Forward Flight," NASA TM-100541, April 1988.

[42]Lim, T. T., "An Experimental Study of a Vortex Ring Interacting with an Inclined Wall," *Experiments in Fluids,* Vol. 7, No. 7, 1989, pp. 453–463.

[43]Quackenbush, T. R., Bliss, D. B., Lam, G., and Katz, A., "New Vortex/Surface Interaction Methods for the Prediction of Wake-Induced Airframe Loads," Second A.R.O. Workshop on Rotorcraft Interactional Aerodynamics, Georgia Inst. of Technology, Atlanta, GA, March 1990.

[44]Martin, R. M., Elliott, J. W., and Hoad, D. R., "Experimental and Analytical Predictions of Rotor Blade Vortex Interaction," *Journal of the American Helicopter Society,* Vol. 31, No. 4, 1986, pp. 12–20.

[45]Leishman, J. G., and Bagai, A., "Shadowgraphic Flow Visualization of a Rotor Wake in Low Speed Forward Flight," VHS Video, Dept. of Aerospace Engineering, Univ. of Maryland, College Park, MD, March 1991 (available from the authors).

[46]Atias, M., and Weihs, D., "Motion of Aircraft Trailing Vortices near the Ground," *Journal of Aircraft,* Vol. 21, No. 10, 1984, pp. 783–786.

[47]Doligalski, T. L., and Walker, J. D. A., "The Boundary Layer Induced by a Convected Two-Dimensional Vortex," *Journal of Fluid Mechanics,* Vol. 139, 1984, pp. 1–28.

[48]Walker, J. D. A., Smith, C. R., Cerra, A. W., and Doligalski, T. L., "The Impact of a Vortex Ring on a Wall," *Journal of Fluid Mechanics,* Vol. 181, 1987, pp. 99–140.

[49]Simons, I. A., Pacifico, R. R., and Jones, J. P., "The Movement, Structure and Breakdown of Trailing Vortices from a Rotor Blade," CAL/USAAVLABS Symposium on Aerodynamic Problems Associated with V/STOL Aircraft, Vol. 1—Propeller and Rotor Aerodynamics, Buffalo, NY, June 22–24, 1966.

[50]Johnson, W., *Helicopter Theory,* Princeton Univ. Press, Princeton, NJ, 1980.